Theory and simulation of anisotropic pair correlations in ferrofluids in magnetic fields

Ekaterina A. Elfimova, Alexey O. Ivanov, and Philip J. Camp

Citation: The Journal of Chemical Physics **136**, 194502 (2012); doi: 10.1063/1.4717718
View online: http://dx.doi.org/10.1063/1.4717718
View Table of Contents: http://scitation.aip.org/content/aip/journal/jcp/136/19?ver=pdfcov
Published by the AIP Publishing

Theory and simulation of anisotropic pair correlations in ferrofluids in magnetic fields

Ekaterina A. Elfimova,[1] Alexey O. Ivanov,[1] and Philip J. Camp[2,a)]
[1]*Institute of Mathematics and Computer Sciences, Ural Federal University, 51 Lenin Avenue, Ekaterinburg 620000, Russia*
[2]*School of Chemistry, University of Edinburgh, West Mains Road, Edinburgh EH9 3JJ, Scotland*

(Received 16 January 2012; accepted 27 April 2012; published online 16 May 2012)

Anisotropic pair correlations in ferrofluids exposed to magnetic fields are studied using a combination of statistical-mechanical theory and computer simulations. A simple dipolar hard-sphere model of the magnetic colloidal particles is studied in detail. A virial-expansion theory is constructed for the pair distribution function (PDF) which depends not only on the length of the pair separation vector, but also on its orientation with respect to the field. A detailed comparison is made between the theoretical predictions and accurate simulation data, and it is found that the theory works well for realistic values of the dipolar coupling constant ($\lambda = 1$), volume fraction ($\varphi \leq 0.1$), and magnetic field strength. The structure factor is computed for wavevectors either parallel or perpendicular to the field. The comparison between theory and simulation is generally very good with realistic ferrofluid parameters. For both the PDF and the structure factor, there are some deviations between theory and simulation at uncommonly high dipolar coupling constants, and with very strong magnetic fields. In particular, the theory is less successful at predicting the behavior of the structure factors at very low wavevectors, and perpendicular Gaussian density fluctuations arising from strongly correlated pairs of magnetic particles. Overall, though, the theory provides reliable predictions for the nature and degree of pair correlations in ferrofluids in magnetic fields, and hence should be of use in the design of functional magnetic materials. © *2012 American Institute of Physics*. [http://dx.doi.org/10.1063/1.4717718]

I. INTRODUCTION

Ferrofluids are made from ferromagnetic particles with diameters of order 10 nm suspended in a carrier liquid. They are highly functional materials, with physical properties that can be controlled by the application of magnetic fields or magnetic-field gradients. Applications of ferrofluids include sealants, heat-conduction media, separation media, gas fluidized beds, and hydraulic car suspensions.[1] Suspensions of suitably functionalized magnetic nanoparticles can also be used for targeted drug delivery, medical diagnosis, and localized cell destruction using field-induced hyperthermia. One of the key characteristics of a ferrofluid is how the microscopic organization of the particles responds to an applied magnetic field, which in turn impacts upon rheology[2] and electromagnetic properties such as optical anisotropy.[3,4] All of these properties can be determined from knowledge of the anisotropy of the interparticle correlations characterized by the pair distribution function (PDF) $g(\boldsymbol{r}_{12})$. Anisotropic, field-induced structure in a colloidal suspension can be locked in to place using chemical gelation, yielding an anisotropic magnetic gel or "ferrogel".[5–7] The properties of ferrogels can also be inferred from knowledge of the field-dependent PDF; in earlier work, this has been achieved by computer simulations,[8,9] but already a more general theory of ferrogel behavior is being developed which requires an analytical PDF as an input.[10]

Field-induced anisotropies in particle correlations have been examined previously by scattering experiments,[11–15] theory,[14,16–20] and computer simulation.[20–23] There are, of course, existing theories for the structures of ferrofluids. In some cases, the particles are strongly interacting (where the characteristic magnetic particle-particle interaction is many times $k_{\mathrm{B}}T$) and hence form chain-like clusters even in the absence of a magnetic field. In these cases, it is assumed at the outset that chain-like clusters exist, and then the theory is developed to take in to account the fluctuations and structure within, and interactions between, the clusters.[16,24–28] Of course, these situations are of interest experimentally,[29] and with regard to the connection between structure[30] and the putative fluid-fluid phase separation in ferromagnetic colloids.[31–34] Although interesting and important, these situations are rather unusual. The interactions in real ferrofluids are typically much weaker, and there have long been theories that address this regime. Jordan studied field-induced structure in dipolar hard spheres (DHSs) using a two-particle theory, and showed that structure is enhanced in the field direction due to chain-like correlations, and suppressed perpendicular to the field direction due to side-by-side parallel repulsions.[16] Hayter and Pynn obtained similar results for the case of perfectly aligned DHSs, studied using the Ornstein-Zernike equation with the mean-spherical approximation (MSA) closure.[17]

a)Author to whom correspondence should be addressed. Electronic mail: philip.camp@ed.ac.uk.

In the current work, a theory for the PDF is constructed using a virial expansion, which offers the possibility of improving the predictions systematically by the addition of extra terms. The key thermodynamic parameters (defined formally in Sec. II) are the volume fraction of magnetic particles φ, and the dipolar coupling constant λ which measures the strength of the magnetic dipole-dipole interactions compared to the thermal energy. Some earlier studies were focused on the PDFs of isotropic ferrofluids with no magnetic field applied; in Refs. 19 and 35, Elfimova and Ivanov developed virial expansions for the PDF with terms of orders up to $\varphi^2\lambda^2$ and $\varphi\lambda^4$. For the case of an applied magnetic field, anisotropic terms of orders up to $\varphi\lambda$ have been calculated.[19,20] The Fourier transform of $g(\boldsymbol{r}_{12})$ yields the static structure factor $S(\boldsymbol{k})$,[36] which has been compared to data from molecular dynamics simulations of dipolar soft-sphere fluids.[20] The comparison showed that the virial expansion at this level provides reasonable predictions for $S(\boldsymbol{k})$ in the ranges $\lambda \lesssim 1$ and $\varphi \lesssim 0.2$, but that improvements are required to achieve a reliable theory. Therefore, the next step is to calculate the anisotropic PDF by determining the field dependence of the term of order $\varphi\lambda^2$ – which is already very complicated to derive – and to add this to the known field-dependent terms of lower order.[19,20] Ideally, field-dependent terms of all orders would be calculated; fortunately, as will be shown below, the theory in its current form is reliable with physically realistic parameters, meaning $\lambda \sim 1$ and $\varphi \leq 0.1$. Note that experimental measurements of structural anisotropy using techniques such as optical birefringence demand that the volume fraction is low (not more than 0.1) in order that the optical transmission is high and multiple scattering can be ignored.

The aims of the current work are: (i) to study the anisotropies in the PDF and the structure factor in DHS fluids, for which the theoretical PDF containing field-dependent terms up to $\mathcal{O}(\varphi\lambda^2)$ can be expressed in closed form; (ii) to test the theoretical predictions against results from Monte Carlo (MC) simulations; and (iii) to emphasize the significance of these results to real ferrofluids. The DHS model is actually a rather good representation for some real ferrofluids. For example, the magnetization curves for a highly polydisperse magnetite ferrofluid were reproduced essentially exactly by a modified mean-field model and computer simulations of a polydisperse DHS fluid.[37,38]

The paper is organized as follows. Section II contains a definition of the DHS model, the interaction potentials, and the thermodynamic parameters. The virial-expansion theory is outlined in Sec. III, and the expansion coefficients are given in detail. Section IV summarizes some simulation details. The results are reported in Sec. V, starting with the PDF, and then moving on to the structure factor. Section VI concludes the paper.

II. MODEL

The ferrofluid is modeled as a DHS fluid of N identical hard spheres of diameter σ, each carrying a central point dipole $\boldsymbol{\mu}$, confined to a volume V, and at temperature T. Under the influence of an external magnetic field, the thermodynamic properties of a magnetic medium are dependent on the shape of the container due to demagnetization effects. Therefore, in theoretical calculations, the container is chosen to be a prolate ellipsoid of revolution of infinite elongation aligned along the field direction; in this case, the demagnetization factor is zero and the internal magnetic field coincides with the external field.

The external magnetic field $\boldsymbol{H} = (0, 0, H)$ is taken to be parallel with the laboratory z axis. The coordinates of particle i are expressed in polar coordinates: the position vector $\boldsymbol{r}_i$ is given in terms of radial distance r_i, polar angle θ_i, and azimuthal angle ϕ_i; the unit vector $\boldsymbol{\Omega}_i$ describes the orientation of its magnetic moment $\boldsymbol{\mu}_i = \mu\boldsymbol{\Omega}_i$ and is given in terms of polar angle ω_i and azimuthal angle ζ_i. The total potential energy of the system $U = U_{\text{int}} + U_{\text{ext}}$ contains contributions from hard-sphere and dipolar particle-particle interactions (U_{int}), and the interactions between the dipoles and the external field (U_{ext}). U_{int} is given by

$$U_{\text{int}} = \sum_{i<j}^{N} u_{ij} = \sum_{i<j}^{N} \left(u_{ij}^{\text{s}} + u_{ij}^{\text{d}}\right), \tag{1}$$

where the hard-sphere interaction potential is

$$u_{ij}^{\text{s}} = \begin{cases} \infty & r_{ij} < \sigma \\ 0 & r_{ij} \geq \sigma \end{cases} \tag{2}$$

and the dipole-dipole interaction potential is

$$u_{ij}^{\text{d}} = \frac{\mu_0}{4\pi}\left[\frac{(\boldsymbol{\mu}_i \cdot \boldsymbol{\mu}_j)}{r_{ij}^3} - \frac{3(\boldsymbol{\mu}_i \cdot \boldsymbol{r}_{ij})(\boldsymbol{\mu}_j \cdot \boldsymbol{r}_{ij})}{r_{ij}^5}\right], \tag{3}$$

where $\boldsymbol{r}_{ij} = \boldsymbol{r}_j - \boldsymbol{r}_i$ is the interparticle separation vector, $r_{ij} = |\boldsymbol{r}_{ij}|$, and $\mu_0 = 4\pi \times 10^{-7}$ H m^{-1} is the vacuum magnetic permeability. The external-field contribution is given by

$$U_{\text{ext}} = -\mu_0 \sum_{i=1}^{N} \boldsymbol{\mu}_i \cdot \boldsymbol{H} = -\mu_0 \mu H \sum_{i=1}^{N} \cos\omega_i. \tag{4}$$

The strength of the interparticle interactions is characterized by the dipolar coupling constant $\lambda = \beta\mu_0\mu^2/4\pi\sigma^3$ where $\beta = 1/k_{\text{B}}T$ and k_{B} is Boltzmann's constant. The particle concentration is expressed as the volume fraction $\varphi = \rho v$, where $\rho = N/V$ is the number density, and $v = \pi\sigma^3/6$ is the particle volume. Finally, the dipole-field interaction is measured by the Langevin parameter $\alpha = \beta\mu_0\mu H$. Typical experimental parameters for real magnetite (Fe_3O_4) ferrofluids are mean diameter $\sigma \sim 10$ nm, saturation magnetization $M_{\text{s}} = 4.8 \times 10^5$ A m^{-1}, and particle dipole moment $\mu = M_{\text{s}}v \sim 10^{-19}$ A m^2. At room temperature ($T = 293$ K) the dipolar coupling constant $\lambda \sim 1$. A typical ferrofluid reaches about 80% of its saturation magnetization when the Langevin parameter $\alpha = 5$; with the above parameters, this corresponds to a magnetic field of $H \sim 100$ kA m^{-1}. Moderately concentrated ferrofluids have volume fractions of order $\varphi \sim 0.1$. Therefore, in this study, systems will be studied with $\lambda = 1$ and 2, and $\alpha = 0$, 1, 2, and 5. Systems with volume fractions $\varphi = 0.1$ and 0.2 are used for detailed tests of the theoretical predictions for the PDF, while volume fractions in the range $0.01 \leq \varphi \leq 0.2$ will be surveyed to provide a general overview

of the structure factor. It is known that with these parameters there is not a significant degree of particle aggregation into distinct chain-like clusters.[20,26] (See, e.g., Fig. 1 of Ref. 8.) Nonetheless, significant dipolar correlations are to be anticipated and are the subject of this study.

III. THEORY

The crucial first step in the theoretical development is the separation of the interaction potential into the external-field dependent term $U_{\rm ext}$, and the interaction term $U_{\rm int}$. This makes it possible to perform a virial expansion starting from the exactly solvable ideal paramagnetic gas where $U_{\rm int} = 0$. The configurational integral for the DHS fluid is written

$$Z = \int \mathrm{d}1 \ldots \int \mathrm{d}N \prod_{i<j}^{N} (1 + f_{ij}), \tag{5}$$

where $f_{ij} = \exp(-\beta u_{ij}) - 1$ is the Mayer function for the particle-particle interaction potential $u_{ij} = u^{\rm s}_{ij} + u^{\rm d}_{ij}$ only. The field-dependent terms are incorporated in to the shorthand notation

$$\int \mathrm{d}i = \int \mathrm{d}\boldsymbol{r}_i \int \exp(\alpha \cos\omega_i)\mathrm{d}\boldsymbol{\Omega}_i,$$

where $\mathrm{d}\boldsymbol{r}_i = r_i^2 \mathrm{d}r_i \sin\theta_i \mathrm{d}\theta_i \mathrm{d}\phi_i$ and $\mathrm{d}\boldsymbol{\Omega}_i = \sin\omega_i \mathrm{d}\omega_i \mathrm{d}\zeta_i$. For the ideal paramagnetic gas, $u_{ij} = 0$ and $Z_{\rm id} = [4\pi V \sinh(\alpha)/\alpha]^N$. The two-particle density is[36]

$$\begin{aligned}\rho(\boldsymbol{r}, \boldsymbol{r}') &= \left\langle \sum_{i=1}^{N} \sum_{j\neq i}^{N} \delta(\boldsymbol{r} - \boldsymbol{r}_i)\delta(\boldsymbol{r}' - \boldsymbol{r}_j) \right\rangle \\ &= \frac{N(N-1)}{Z} \int \exp(\alpha \cos\omega_1)\mathrm{d}\boldsymbol{\Omega}_1 \\ &\quad \times \int \exp(\alpha \cos\omega_2)\mathrm{d}\boldsymbol{\Omega}_2 \\ &\quad \times \int \mathrm{d}3 \ldots \int \mathrm{d}N \prod_{i<j}^{N} (1 + f_{ij}).\end{aligned} \tag{6}$$

For the ideal paramagnetic gas, the two-particle density is $\rho_{\rm id}(\boldsymbol{r}, \boldsymbol{r}') = N(N-1)/V^2 \approx \rho^2$. The PDF is defined as[36]

$$g(\boldsymbol{r}_1, \boldsymbol{r}_2) = \frac{\rho(\boldsymbol{r}_1, \boldsymbol{r}_2)}{\rho^2}. \tag{7}$$

The fluid is homogeneous and so the PDF is dependent only on the separation vector $\boldsymbol{r}_2 - \boldsymbol{r}_1$, i.e., $g(\boldsymbol{r}_1, \boldsymbol{r}_2) = g(0, \boldsymbol{r}_2 - \boldsymbol{r}_1) \equiv g(\boldsymbol{r}_{12})$. Furthermore, the fluid in an applied field possesses cylindrical symmetry and so the PDF depends only on the separation r_{12} and on the angle $\theta = \angle(\boldsymbol{r}_{12}, \boldsymbol{H})$, i.e., it may be written as $g(r_{12}, \theta)$. In zero field, the fluid is homogeneous and isotropic and therefore the PDF is $g(r_{12})$, which depends only on the distance r_{12}. For the ideal paramagnetic gas, $g(\boldsymbol{r}_{12}) = 1$. Finally, all distances may be expressed in the dimensionless form $x = r_{12}/\sigma$. The equivalent notations $g(\boldsymbol{r}_{12})$ and $g(x, \theta)$ for the anisotropic PDF in a field will be used interchangeably.

A. Virial expansion

The PDF may be determined using a virial expansion in terms of the volume fraction φ,

$$g(\boldsymbol{r}_{12}) = \sum_{k=2}^{\infty} \varphi^{k-2} B_k(\boldsymbol{r}_{12}). \tag{8}$$

Here, $B_k(\boldsymbol{r}_{12})$ is a type of virial coefficient that may be expressed in terms of Mayer functions.[36,39,40] For instance, the first two terms are

$$B_2(\boldsymbol{r}_{12}) = \langle f_{12} + 1 \rangle_{\boldsymbol{\Omega}_1, \boldsymbol{\Omega}_2}, \tag{9}$$

$$B_3(\boldsymbol{r}_{12}) = \frac{1}{v} \int \mathrm{d}\boldsymbol{r}_3 \, \langle (f_{12} + 1) f_{13} f_{23} \rangle_{\boldsymbol{\Omega}_1, \boldsymbol{\Omega}_2, \boldsymbol{\Omega}_3}, \tag{10}$$

where the angled brackets denote an average over the orientational distribution function of the ideal paramagnetic gas

$$\langle \ldots \rangle_{\boldsymbol{\Omega}} = \frac{\alpha}{4\pi \sinh(\alpha)} \int \exp(\alpha \cos\omega) \mathrm{d}\boldsymbol{\Omega}. \tag{11}$$

The coefficients $B_k(\boldsymbol{r}_{12})$ are themselves functions of the dipolar coupling constant λ, which for a real ferrofluid is of order 1. Therefore, $B_k(\boldsymbol{r}_{12})$ may be expanded in terms of a power series in λ. This is achieved by splitting the Mayer function in to separate terms reflecting the hard-sphere and dipolar interaction potentials. Defining the hard-sphere and dipolar Mayer functions as $f^{\rm s}_{ij} = \exp(-\beta u^{\rm s}_{ij}) - 1$ and $f^{\rm d}_{ij} = \exp(-\beta u^{\rm d}_{ij}) - 1$, respectively, the total Mayer function may be written

$$f_{ij} = f^{\rm s}_{ij} + \left(f^{\rm s}_{ij} + 1\right) f^{\rm d}_{ij} = f^{\rm s}_{ij} + \left(f^{\rm s}_{ij} + 1\right) \sum_{l=1}^{\infty} \frac{\left(-\beta u^{\rm d}_{ij}\right)^l}{l!}, \tag{12}$$

where $f^{\rm d}_{ij}$ has been expanded as a Taylor series in which the "small parameter" will be the dipolar coupling constant λ. Using the expansion (12) for the evaluation of B_k, and collecting together all terms of equal orders in φ and λ gives

$$\begin{aligned} g(\mathbf{r}_{12}) &= \sum_{k=0}^{\infty} \sum_{l=0}^{\infty} \varphi^k \lambda^l \beta_{kl}(\boldsymbol{r}_{12}) \\ &= g_{\rm s}(r_{12}) + \sum_{k=0}^{\infty} \sum_{l=1}^{\infty} \varphi^k \lambda^l \beta_{kl}(\boldsymbol{r}_{12}). \end{aligned} \tag{13}$$

The hard-sphere PDF is given by the sum of terms with $l = 0$,

$$g_{\rm s}(r_{12}) = \sum_{k=0}^{\infty} \varphi^k \beta_{k0}(r_{12}), \tag{14}$$

and is taken as known in some convenient form. In the present work, the Percus-Yevick hard-sphere PDF is used.[36]

B. Zero-field PDF expansion coefficients

Calculations for the DHS fluid in zero field up to terms of order $\varphi^2\lambda^2$ were presented in Ref. 35. Explicit expressions were given for $\beta_{02}(x)$, $\beta_{12}(x)$, and $\beta_{22}(x)$, and it was shown

TABLE I. Expansion coefficients $\beta_{kl}(x)$ for the case of zero field (from Refs. 19 and 35), and functions $\gamma_{kl}(x)$ for the case of non-zero field. Each of the functions is equal to zero for $x < 1$.

Coefficient	Range	Formula
$\beta_{02}(x)$	$x \geq 1$	$\frac{1}{3x^6}$
$\beta_{12}(x)$	$1 \leq x < 2$	$\frac{(x-1)}{6x^6(x+1)^3}(6x^9+8x^8-16x^7-40x^6$ $-39x^5-36x^4-45x^3-64x^2-52x-16)$
	$x \geq 2$	$-\frac{16}{3(x^2-1)^3}$
$\gamma_{01}(x)$	$x \geq 1$	$\frac{2}{x^3}$
$\gamma_{11}(x)$	$1 \leq x < 2$	$x^3-6x+1-\frac{12}{x^2}+\frac{16}{x^3}$
	$x \geq 2$	$-\frac{32}{x^3}$
$\gamma_{02}(x)$	$x \geq 1$	$\frac{1}{x^6}$

that in zero field, the coefficients $\beta_{01}(x)$, $\beta_{03}(x)$, $\beta_{11}(x)$, and $\beta_{21}(x)$ are all equal to zero. It was shown that the virial expansion of $g(r_{12})$, incorporating dipolar terms up to order $\varphi^2\lambda^2$ and $g_s(r_{12})$ with terms up to order φ^2, was valid for weakly interacting particles ($\lambda \sim 1$) and volume concentrations up to $\varphi \simeq 0.30$. Methods of calculating higher order terms were suggested in Ref. 19, and explicit calculations of $\beta_{04}(x)$, $\beta_{13}(x)$, and $\beta_{14}(x)$ were performed. It was also shown that the dipole-dipole interaction is somewhat capricious in its effects on the correlations: its contributions to the PDF of even powers (λ^2, λ^4) indicate an effective interparticle attraction, whereas those proportional to λ^3 indicate an effective interparticle repulsion. The expressions for coefficients $\beta_{kl}(x)$ up to $k = 1$ and $l = 2$ are given in Table I, as they will be referred to in what follows. An important feature of the zero-field coefficients is that the asymptotic decay is proportional to x^{-6} or faster, and hence the correlations are short ranged.

C. Field-dependent PDF expansion coefficients

In an applied field, the PDF and expansion coefficients depend on both x and the angle θ. The extension of the theory to non-zero field was first attempted in Refs. 19 and 20, where calculations of the anisotropic functions $\beta_{01}(x, \theta)$ and $\beta_{11}(x, \theta)$ were presented (recall that these coefficients disappear in zero field). A comparison of the theory (modified for a soft-sphere repulsion rather than a hard-sphere repulsion) with the results from molecular dynamics simulations of a dipolar soft-sphere fluid showed that the field-induced anisotropy in the structure factor was predicted somewhat accurately for $\lambda = 1$ up to $\varphi = 0.25$, and for $\lambda = 1.5$ up to $\varphi = 0.15$. Here, the coefficients $\beta_{kl}(x, \theta)$ up to $k = 1$ and $l = 2$ are presented. Already, these are lengthy calculations involving three-body interactions with the dipolar terms included up to order λ^2. Due to the symmetry of the fluid, it is convenient to express the PDF in terms of spherical Legendre polynomials $P_n(\cos\theta)$. The lowest order anisotropic terms are proportional to $P_2(z) = (3z^2 - 1)/2$,[19]

$$\beta_{01}(x, \theta) = L^2(\alpha)P_2(\cos\theta)\gamma_{01}(x), \tag{15}$$

$$\beta_{11}(x, \theta) = L^2(\alpha)P_2(\cos\theta)\gamma_{11}(x). \tag{16}$$

The field dependence is given by the Langevin function $L(\alpha) = \coth\alpha - 1/\alpha$; it is squared because of averaging over the orientations of the two magnetic moments $\mu\mathbf{\Omega}_1$ and $\mu\mathbf{\Omega}_2$. The functions $\gamma_{kl}(x)$ are collected in Table I. These terms reflect the long-range nature of the dipole-dipole interactions, decaying asymptotically as x^{-3}. Since $L(0) = 0$, both $\beta_{01}(x)$ and $\beta_{11}(x)$ vanish in zero field.[35]

$\beta_{01}(x, \theta)$ and $\beta_{11}(x, \theta)$ are the coefficients of terms of order λ and $\varphi\lambda$, respectively, and truncation at this level is only accurate for low values of $\lambda < 1$. To improve the accuracy of the theory requires calculation of the terms $\beta_{02}(x, \theta)$ and $\beta_{12}(x, \theta)$. $\beta_{02}(x, \theta)$ arises from substituting the $l = 2$ term from Eq. (12) in to Eq. (9),

$$\beta_{02}(\boldsymbol{r}_{12}) = \frac{\left(f_{12}^{s}+1\right)}{2}\left\langle\left(\frac{\beta u_{12}^{d}}{\lambda}\right)^2\right\rangle_{\mathbf{\Omega}_1,\mathbf{\Omega}_2}. \tag{17}$$

Performing the orientational averages over $\mathbf{\Omega}_1$ and $\mathbf{\Omega}_2$ yields

$$\begin{aligned}\beta_{02}(x, \theta) = \Bigg\{&\frac{36}{35}L_3^2(\alpha)P_4(\cos\theta)\\ &+\frac{2}{3}L_3(\alpha)\left[1-\frac{L_3(\alpha)}{7}\right]P_2(\cos\theta)\\ &+\frac{1}{3}\left[1+\frac{L_3^2(\alpha)}{5}\right]\Bigg\}\gamma_{02}(x),\end{aligned} \tag{18}$$

where $P_4(z) = (35z^4 - 30z^2 + 3)/8$ is the fourth Legendre polynomial, $\gamma_{02}(x)$ is given in Table I, and the field-dependence is expressed with the function

$$L_n(\alpha) = 1 - \frac{nL(\alpha)}{\alpha}. \tag{19}$$

Here, $L_n(\alpha)$ has the properties $L_n(0) = 1 - n/3$ and $\lim_{\alpha\to\infty} L_n(\alpha) = 1$. For zero field ($\alpha = 0$), substituting $L_3(0) = 0$ in to Eq. (18) confirms that $\beta_{02}(x) = \gamma_{02}(x)/3$ coincides with the isotropic function derived in Ref. 35 and listed in Table I. For the case of perfect alignment ($\alpha \to \infty$), Eq. (18) is proportional to $(3\cos^2\theta - 1)^2/x^6$ which is clearly just the dipolar factor from Eq. (17).

The next most important field-dependent coefficient is $\beta_{12}(x, \theta)$, which consists of the four three-body terms representing various interactions of order λ^2,

$$\beta_{12}(\boldsymbol{r}_{12}) = I_1(\boldsymbol{r}_{12}) + 2I_2(\boldsymbol{r}_{12}) + I_3(\boldsymbol{r}_{12}) + 2I_4(\boldsymbol{r}_{12}), \tag{20}$$

$$I_1(\boldsymbol{r}_{12}) = \frac{(f_{12}^{\rm s}+1)}{2v}\int {\rm d}\boldsymbol{r}_3 f_{13}^{\rm s} f_{23}^{\rm s}\left\langle\left(\frac{\beta u_{12}^{\rm d}}{\lambda}\right)^2\right\rangle_{\boldsymbol{\Omega}_1,\boldsymbol{\Omega}_2}, \quad (21)$$

$$I_2(\boldsymbol{r}_{12}) = \frac{(f_{12}^{\rm s}+1)}{2v}\int {\rm d}\boldsymbol{r}_3 (f_{13}^{\rm s}+1) f_{23}^{\rm s}\left\langle\left(\frac{\beta u_{13}^{\rm d}}{\lambda}\right)^2\right\rangle_{\boldsymbol{\Omega}_1,\boldsymbol{\Omega}_3}, \quad (22)$$

$$I_3(\boldsymbol{r}_{12}) = \frac{(f_{12}^{\rm s}+1)}{v}\int {\rm d}\boldsymbol{r}_3 (f_{13}^{\rm s}+1)(f_{23}^{\rm s}+1) \times\left\langle\left(\frac{\beta^2 u_{13}^{\rm d} u_{23}^{\rm d}}{\lambda^2}\right)\right\rangle_{\boldsymbol{\Omega}_1,\boldsymbol{\Omega}_2\boldsymbol{\Omega}_3}, \quad (23)$$

$$I_4(\boldsymbol{r}_{12}) = \frac{(f_{12}^{\rm s}+1)}{v}\int {\rm d}\boldsymbol{r}_3 (f_{13}^{\rm s}+1) f_{23}^{\rm s}\left\langle\left(\frac{\beta^2 u_{13}^{\rm d} u_{12}^{\rm d}}{\lambda^2}\right)\right\rangle_{\boldsymbol{\Omega}_1,\boldsymbol{\Omega}_2\boldsymbol{\Omega}_3}. \quad (24)$$

The function $I_1(x,\theta)$ is equal to $\beta_{02}(x,\theta)$ modified by a simple isotropic factor $h_1(x)$ which is given in Table II,

$$I_1(x,\theta) = \beta_{02}(x,\theta) h_1(x). \quad (25)$$

To evaluate $I_2(x,\theta)$, the first step is to average over the orientations $\boldsymbol{\Omega}_1$ and $\boldsymbol{\Omega}_3$, which leads to

$$\left\langle\left(\frac{\beta u_{13}^{\rm d}}{\lambda}\right)^2\right\rangle_{\boldsymbol{\Omega}_1,\boldsymbol{\Omega}_3} = \frac{2}{x_{13}^6}\left\{\frac{36}{35}L_3^2(\alpha)P_4(\boldsymbol{e}_{13}\cdot\boldsymbol{z}) + \frac{2}{3}L_3(\alpha)\left[1-\frac{L_3(\alpha)}{7}\right]P_2(\boldsymbol{e}_{13}\cdot\boldsymbol{z}) + \frac{1}{3}\left[1+\frac{L_3^2(\alpha)}{5}\right]\right\}, \quad (26)$$

where $\boldsymbol{e}_{13}$ is a unit vector parallel to $\boldsymbol{r}_{13} = \boldsymbol{r}_3 - \boldsymbol{r}_1$, $\boldsymbol{z} = (0,0,1)$ is the laboratory z axis and field direction, and $x_{13} = |\boldsymbol{r}_{13}|/\sigma$. Next, the integration over $\boldsymbol{r}_3$ is replaced by one over $\boldsymbol{r}_{13}$ with particle 1 at the origin. The factor $(f_{13}^{\rm s}+1)$ in Eq. (22) restricts the domain of integration to $r_{13} \geq \sigma$. Similarly, the factor $f_{23}^{\rm s}$ means that particle 3 must be within a distance σ of particle 2. The subsequent integrations are performed by using a new frame in which $\boldsymbol{r}_{12}$ is parallel with the polar axis (z'); the geometry is illustrated in Fig. 1. If particles 1 and 2 lie in the xz and $x'z'$ planes of the laboratory and new frames, respectively, then the laboratory z axis in the new frame is $\boldsymbol{z} = (-\sin\theta, 0, \cos\theta)$ (remembering that θ is the angle between $\boldsymbol{r}_{12}$ and the laboratory z axis). Setting $\boldsymbol{e}_{13} = (\sin\theta_{13}\cos\phi_{13}, \sin\theta_{13}\sin\phi_{13}, \cos\theta_{13})$ in the new frame, the integration of the Legendre polynomials over the azimuthal angle ϕ_{13} gives

$$\int_0^{2\pi} P_n(\boldsymbol{e}_{13}\cdot\boldsymbol{z}){\rm d}\phi_{13} = 2\pi P_n(\cos\theta)P_n(\cos\theta_{13}) \quad (n=2,4). \quad (27)$$

Now the integrations over θ_{13} and x_{13} can be performed to yield

$$I_2(x,\theta) = L_3^2(\alpha)P_4(\cos\theta)h_{24}(x) + L_3(\alpha)\left[1-\frac{L_3(\alpha)}{7}\right]P_2(\cos\theta)h_{22}(x) + \left[1+\frac{L_3^2(\alpha)}{5}\right]h_{20}(x), \quad (28)$$

where the functions $h_{24}(x)$, $h_{22}(x)$, and $h_{20}(x)$ are given in Table II. The calculation of $I_3(x,\theta)$ proceeds in a similar way. First, averaging over $\boldsymbol{\Omega}_1$, $\boldsymbol{\Omega}_2$, and $\boldsymbol{\Omega}_3$ gives

$$\left\langle\frac{\beta^2 u_{13}^{\rm d} u_{23}^{\rm d}}{\lambda^2}\right\rangle = \frac{L^2(\alpha)}{x_{13}^3 x_{23}^3}\left\{\frac{9L(\alpha)}{\alpha}(\boldsymbol{e}_{13}\cdot\boldsymbol{z})(\boldsymbol{e}_{23}\cdot\boldsymbol{z}) \times[(\boldsymbol{e}_{13}\cdot\boldsymbol{e}_{23}) - (\boldsymbol{e}_{13}\cdot\boldsymbol{z})(\boldsymbol{e}_{23}\cdot\boldsymbol{z})] + 4L_2(\alpha)P_2(\boldsymbol{e}_{13}\cdot\boldsymbol{z})P_2(\boldsymbol{e}_{23}\cdot\boldsymbol{z})\right\}, \quad (29)$$

where $\boldsymbol{e}_{23}$ is a unit vector parallel to $\boldsymbol{r}_{23} = \boldsymbol{r}_3 - \boldsymbol{r}_2$, and $L_2(\alpha)$ is defined in Eq. (19). The next step is an integration over $\boldsymbol{r}_{13}$, which is performed in the frame shown in Fig. 1. In this frame, the vector $\boldsymbol{r}_{23} = \boldsymbol{r}_{13} - \boldsymbol{r}_{12}$ has coordinates $(r_{13}\sin\theta_{13}\cos\phi_{13}, r_{13}\sin\theta_{13}\sin\phi_{13}, r_{13}\cos\theta_{13} - r_{12})$, and $x_{23} = r_{23}/\sigma$. Performing the integrations over θ_{13}, ϕ_{13}, and x_{13} yields

$$I_3(x,\theta) = L^2(\alpha)\left\{L_3(\alpha)P_4(\cos\theta)h_{34}(x) + \left[4-\frac{5L(\alpha)}{\alpha}\right] \times P_2(\cos\theta)h_{32}(x) + \left[2-\frac{L(\alpha)}{\alpha}\right]h_{30}(x)\right\}, \quad (30)$$

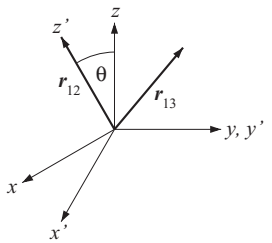

FIG. 1. Laboratory frame (x, y, z) and shifted frame (x', y', z') for the calculation of I_3 and I_4 described in Sec. III C. $\boldsymbol{r}_{ij} = \boldsymbol{r}_j - \boldsymbol{r}_i$ is the separation vector between particles i and j.

TABLE II. Expansion coefficients $h_i(x)$ and $h_{ij}(x)$ for the calculation of $\beta_{12}(x,\theta)$ in non-zero field. Each of the functions is equal to zero for $x < 1$.

Coefficient	Range	Formula
$h_1(x)$	$1 \le x < 2$	$8 - 6x + \frac{x^3}{2}$
	$x \ge 2$	0
$h_{24}(x)$	$1 \le x < 2$	$-\frac{27(x^2+7)}{112x^5}\ln(x+1)$ $+\frac{9(x+2)}{4480x^4(x+1)^3}(21x^{11}+21x^{10}-104x^9-146x^8+35x^7+159x^6$ $+54x^5+64x^4+50x^3+410x^2+840x+420)$
	$x \ge 2$	$-\frac{27(x^2+7)}{112x^5}\ln\left(\frac{x+1}{x-1}\right)+\frac{9(15x^6-191x^4+265x^2-105)}{280x^4(x^2-1)^3}$
$h_{22}(x)$	$1 \le x < 2$	$\frac{1}{2x^3}\ln(x+1)+\frac{(x+2)}{24x^2(x+1)^3}(2x^7+2x^6-7x^5$ $-11x^4-11x^3-5x^2-12x-6)$
	$x \ge 2$	$\frac{1}{2x^3}\ln\left(\frac{x+1}{x-1}\right)-\frac{3x^4+8x^2-3}{3x^2(x^2-1)^3}$
$h_{20}(x)$	$1 \le x < 2$	$\frac{x(3x^3+x^2-12x-12)}{6(x+1)^3}$
	$x \ge 2$	$-\frac{8}{3(x^2-1)^3}$
$h_{34}(x)$	$1 \le x < 2$	$\frac{9x(x^2+8)}{140}$
	$x \ge 2$	$\frac{288(5x^2-14)}{35x^5}$
$h_{32}(x)$	$1 \le x < 2$	$\frac{1}{14}x(x^2-6)$
	$x \ge 2$	$-\frac{16}{7x^3}$
$h_{30}(x)$	$1 \le x < 2$	$\frac{1}{5}(x+4)(x-2)^2$
	$x \ge 2$	0
$h_4(x)$	$1 \le x < 2$	$\frac{1}{2}-\frac{3}{x^2}$
	$x \ge 2$	$-\frac{16}{x^6}$

where $h_{34}(x)$, $h_{32}(x)$, and $h_{30}(x)$ are given in Table II. $I_4(x,\theta)$ is calculated in analogous fashion. Averaging over $\mathbf{\Omega}_1$, $\mathbf{\Omega}_2$, and $\mathbf{\Omega}_3$ gives

$$\left\langle \frac{\beta^2 u_{13}^{\mathrm{d}} u_{12}^{\mathrm{d}}}{\lambda^2} \right\rangle = \frac{L^2(\alpha)}{x_{13}^3 x_{12}^3}\left\{ \frac{9L(\alpha)}{\alpha}(\boldsymbol{e}_{13}\cdot\boldsymbol{z})(\boldsymbol{e}_{12}\cdot\boldsymbol{z}) \times[(\boldsymbol{e}_{13}\cdot\boldsymbol{e}_{12})-(\boldsymbol{e}_{13}\cdot\boldsymbol{z})(\boldsymbol{e}_{12}\cdot\boldsymbol{z})] + 4L_2(\alpha)P_2(\boldsymbol{e}_{13}\cdot\boldsymbol{z})P_2(\boldsymbol{e}_{12}\cdot\boldsymbol{z})\right\}. \quad (31)$$

Integrations over θ_{13}, ϕ_{13}, and r_{13} yield

$$I_4(x,\theta) = L^2(\alpha)\left\{\frac{36}{35}L_3(\alpha)P_4(\cos\theta)+\frac{1}{3}\left[1+\frac{5L_3(\alpha)}{7}\right] \times P_2(\cos\theta)+\frac{1}{3}\left[1+\frac{L_3(\alpha)}{5}\right]\right\}h_4(x), \quad (32)$$

where $h_4(x)$ is given in Table II. In zero field, $L(\alpha) = L_3(\alpha) = 0$, and hence $I_1(x) = \beta_{02}(x)h_1(x)$, $I_2(x) = h_{20}(x)$, and $I_3(x) = I_4(x) = 0$. Substituting these limiting functions in to Eq. (24) leads to the correct zero-field result for $\beta_{12}(x)$ given in Table I.

To summarize, the PDF is approximated by the sum

$$g(x,\theta) \simeq g_{\mathrm{s}}(x) + \beta_{01}(x,\theta)\lambda + \beta_{02}(x,\theta)\lambda^2 + \beta_{11}(x,\theta)\varphi\lambda + \beta_{12}(x,\theta)\varphi\lambda^2, \quad (33)$$

where $g_{\mathrm{s}}(r_{12})$ is the hard-sphere PDF in some suitable form; the Percus-Yevick result is used in this work. The field dependence (dependence on α) has been determined in the coefficients up to $\beta_{12}(x,\theta)$. The higher order coefficients $\beta_{04}(x)$, $\beta_{13}(x)$, and $\beta_{14}(x)$ are available for the zero-field case. In earlier work[20] they were added to the field-dependent PDF, but it turns out that their contributions to the PDF are negligible. They are omitted here so that the field dependence of the retained terms is exact. The contributions of higher order terms will be discussed further in Sec. VI.

Structure factors at wavevectors perpendicular ($k_\perp$) and parallel ($k_\parallel$) to the field direction were calculated using the following relations, best expressed in cylindrical polar coordinates:

$$S(k_\perp) = 1 + 4\pi\rho\int_0^\infty R\mathrm{d}R\int_0^\infty \mathrm{d}Z\, J_0(k_\perp R)[g(x,\theta)-1], \quad (34)$$

$$S(k_\parallel) = 1 + 4\pi\rho\int_0^\infty R\mathrm{d}R\int_0^\infty \mathrm{d}Z\cos(k_\parallel Z)[g(x,\theta)-1]. \quad (35)$$

Here $x\sigma = \sqrt{R^2+Z^2}$, $\cos\theta = Z/\sqrt{R^2+Z^2}$, and J_0 is a Bessel function of the first kind. The hard-sphere structure factor was calculated analytically from the Ornstein-Zernike

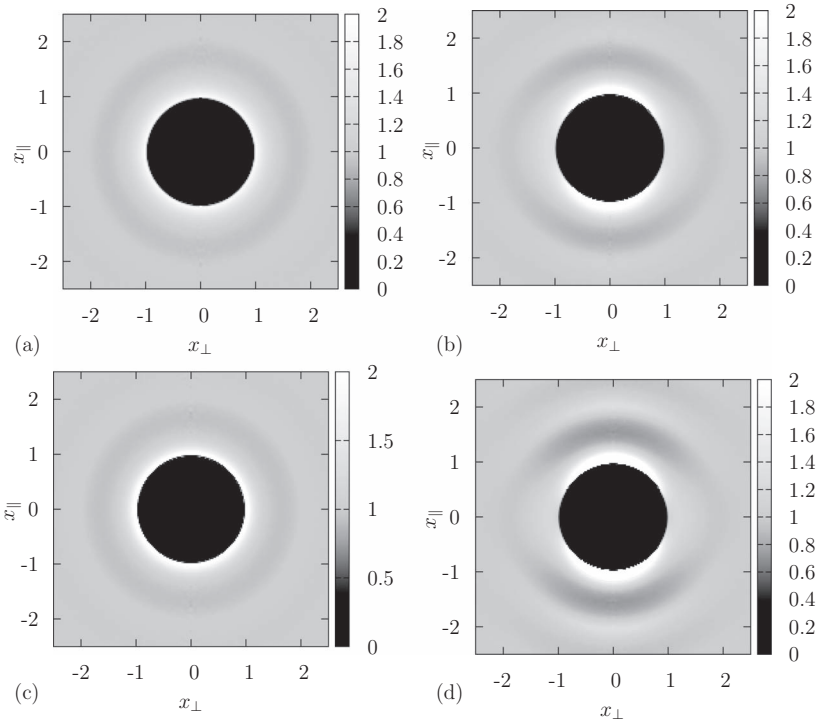

FIG. 2. Pair distribution functions $g(\boldsymbol{r}_{12}) = g(x, \theta)$ calculated in MC simulations of DHS fluids with $\varphi = 0.2$: (a) $\lambda = 1$ and $\alpha = 0$; (b) $\lambda = 1$ and $\alpha = 5$; (c) $\lambda = 2$ and $\alpha = 0$; (d) $\lambda = 2$ and $\alpha = 5$. The horizontal axis is $x_\perp = x \sin\theta$ and the vertical axis is $x_\parallel = x \cos\theta$, where θ is the angle of $\boldsymbol{r}_{12}$ with respect to the field.

equation and the Fourier transform of the Percus-Yevick direct correlation function,[36] and the integrations of the terms arising from dipolar interactions in Eq. (33) were carried out numerically over the range $x \geq 1$. Carrying out the integrals in cylindrical polar coordinates leads to convergent results.[41]

IV. SIMULATIONS

The MC simulations were performed on systems of $N = 500$ DHSs in a cubic box of side L. The long-range dipolar interactions were evaluated using Ewald summation, with conducting boundary conditions to eliminate demagnetization effects.[42] One MC cycle consisted of N attempted translations or rotations per particle, all selected at random. The maximum displacement parameters were set to give acceptance rates of 20% for translations and 50% for rotations. For each value of φ, λ, and α the simulation consisted of 10^6 MC cycles after equilibration. The PDF was calculated on a two-dimensional grid of distances perpendicular and parallel to the applied field ($x_\perp$ and $x_\parallel$, respectively), with an appropriate average over the azimuthal angle in the perpendicular case. Structure factors were computed separately for wavevectors perpendicular and parallel to the field, i.e., $\boldsymbol{k}_\perp = (2\pi/L)(n_x, n_y, 0)$ and $\boldsymbol{k}_\parallel = (2\pi/L)(0, 0, n_z)$ with n_x, n_y, $n_z = 0, \pm1, \pm2, \ldots$. For wavevector $\boldsymbol{k}$,

$$S(\boldsymbol{k}) = \frac{1}{N} \langle \rho_{\boldsymbol{k}} \rho_{-\boldsymbol{k}} \rangle , \tag{36}$$

where $\rho_{\boldsymbol{k}} = \sum_{i=1}^{N} \exp(-\mathrm{i}\boldsymbol{k} \cdot \boldsymbol{r}_i)$ is a Fourier component of the one-particle density. The structure factors were averaged over wavevectors of equal magnitude $k_\perp = |\boldsymbol{k}_\perp|$ and $k_\parallel = |\boldsymbol{k}_\parallel|$.

V. RESULTS

A. Pair distribution function $g(r_{12})$

First of all, to set the scene, Fig. 2 shows grayscale maps of the PDF for DHS fluids with $\varphi = 0.2$, $\lambda = 1$ and 2, and $\alpha = 0$ and 5. The results are plotted in terms of the components of x perpendicular and parallel to the field direction. In zero field ($\alpha = 0$) the PDF is isotropic, and shows short-range attractive correlations for particles close to contact ($x \simeq 1$) and longer range repulsive correlations at $x \simeq 1.5$; this is typical for a moderate-density simple fluid. In a strong, non-zero field ($\alpha = 5$) the fractional magnetizations with $\lambda = 1$ and 2 are 0.835 and 0.854, respectively. (The theoretical description of the magnetization curves and magnetic susceptibilities of real ferrofluids has been discussed in depth in Refs. 37 and 38.) The PDF shows pronounced anisotropy, with a strong enhancement of attractive correlations close to contact in the field direction, and a loss of attractive correlations close to contact in the perpendicular direction. There are also more pronounced repulsive correlations in the field direction in the region of $x_\parallel \simeq 1.5$, and weak attractive correlations appearing in the region of $x_\parallel \simeq 2$. These results correspond to chain-like, nose-to-tail correlations being induced in the field direction. This is a well-known phenomenon and is easy to understand in qualitative terms, but now the quantitative accuracy of the virial expansion theory is to be tested. To this end, attention will be paid to the PDF in the directions parallel and perpendicular to the field, given by $g(x, \theta = 0)$ and $g(x, \theta = \pi/2)$, respectively.

Figure 3 shows $g(x, 0)$ and $g(x, \pi/2)$ for DHS fluids with $\varphi = 0.1$, $\lambda = 1$, and $\alpha = 0$, 1, 2, and 5, from both MC simulations and the virial-expansion theory. [Note that in each panel

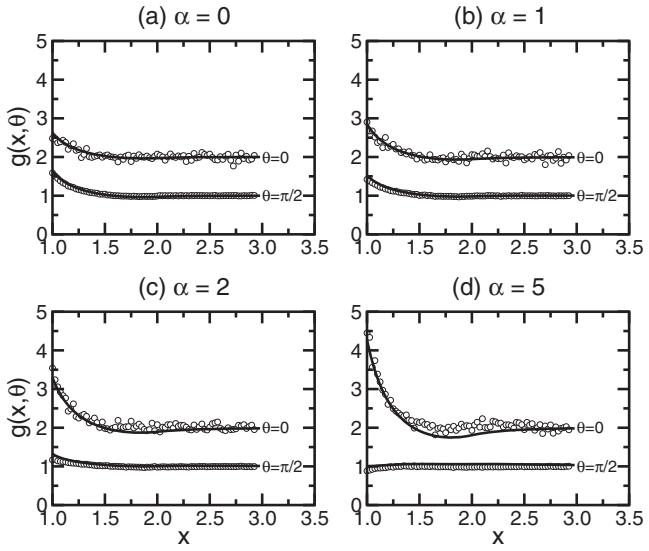

FIG. 3. Pair distribution functions $g(x, \theta)$ parallel to the field ($\theta = 0$, shifted along the ordinate by one unit, for clarity) and perpendicular to the field ($\theta = \pi/2$) in DHS fluids with $\varphi = 0.1$, $\lambda = 1$, and (a) $\alpha = 0$, (b) $\alpha = 1$, (c) $\alpha = 2$, and (d) $\alpha = 5$. The points are from simulations, and the lines are from theory.

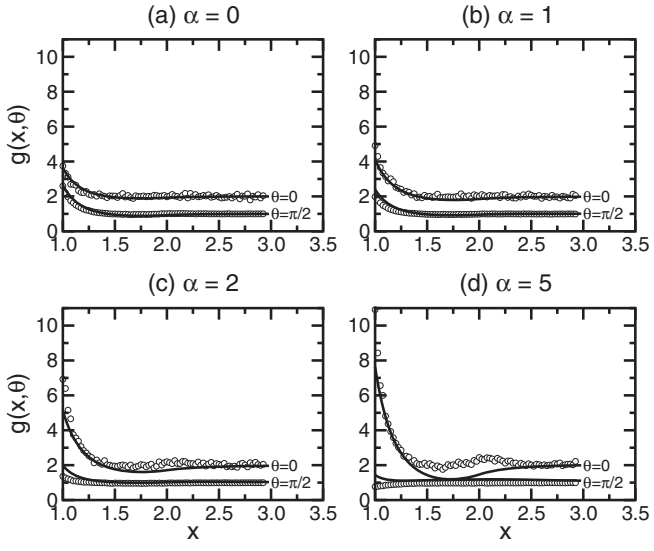

FIG. 4. Pair distribution functions $g(x, \theta)$ parallel to the field ($\theta = 0$, shifted along the ordinate by one unit, for clarity) and perpendicular to the field ($\theta = \pi/2$) in DHS fluids with $\varphi = 0.1$, $\lambda = 2$, and (a) $\alpha = 0$, (b) $\alpha = 1$, (c) $\alpha = 2$, and (d) $\alpha = 5$. The points are from simulations, and the lines are from theory.

of Figs. 3–6, $g(x, 0)$ is shifted up by one unit for clarity; $g(x, \theta) \to 1$ as $x \to \infty$.] In zero field ($\alpha = 0$) the correlations in each direction are equivalent. The theory provides an excellent description of the PDF, getting both the contact value and the decay correct. As the field strength is increased ($\alpha = 1$–5), the contact value of $g(x, 0)$ increases due to the enhanced nose-to-tail correlations between particles in the field direction. Meanwhile, the contact value of $g(x, \pi/2)$ decreases due to the repulsive side-by-side interactions between parallel dipoles aligned with the field. The agreement between theory and simulation is rather good, with significant deviations becoming apparent only in $g(x, 0)$ at $\alpha = 5$ and in the region of $x = 2$. Figure 4 shows the corresponding results for DHS fluids with $\varphi = 0.1$ and $\lambda = 2$. Qualitatively, the simulation results are the similar to those with $\lambda = 1$, except that in zero field ($\alpha = 0$) the short-range correlations are more pronounced, and that in applied fields ($\alpha = 1$–5) there is a greater degree of enhancement in the nose-to-tail correlations as signaled by a greater value of $g(x, 0)$ at contact, and a more pronounced secondary peak in $g(x, 0)$ in the region of $x = 2$. Although the theory appears accurate at $\alpha = 0$ and 1, there are some slight discrepancies at $\alpha = 2$ and 5; specifically, it does not reproduce the second peak in $g(x, 0)$, and it does not predict the downturn in $g(x, \pi/2)$ close to contact between $\alpha = 2$ and $\alpha = 5$. Nonetheless, the overall agreement is quite good, with the most significant features [such as $g(x, 0)$ close to contact] being described very well by the theory.

Figures 5 and 6 show the corresponding results for $g(x, \theta)$ in DHS fluids at volume fraction $\varphi = 0.2$ and with $\lambda = 1$ and $\lambda = 2$, respectively. In general terms, the trends in $g(x, 0)$ and $g(x, \pi/2)$ with increasing α are as discussed above, except of course the degree of correlation is higher due to the higher particle concentration; the simulation results show that there is more pronounced structure, particularly in the peaks near $x = 1$ and $x = 2$. What is more significant is the deviation between theory and simulation when α and/or λ are high. In zero field, the theory does a reasonable job for the isotropic PDF. With $\lambda = 1$, the theory does quite well even up to $\alpha = 2$, but at $\alpha = 5$ there is a significant over-expression of the local minimum in $g(x, 0)$ in the range $1.5 \leq x \leq 2$. With $\lambda = 2$ there are pronounced deviations between simulation and theory at all field strengths.

The fact that the discrepancy between simulation and theory becomes really significant only at the highest volume fraction studied shows that the next-highest order terms in the virial expansion may be sufficient to achieve good accuracy. The next contributions to be included in Eq. (33) are four-body terms of order φ^2. In weak fields, where the particles are not orientationally aligned very strongly, it is likely that terms

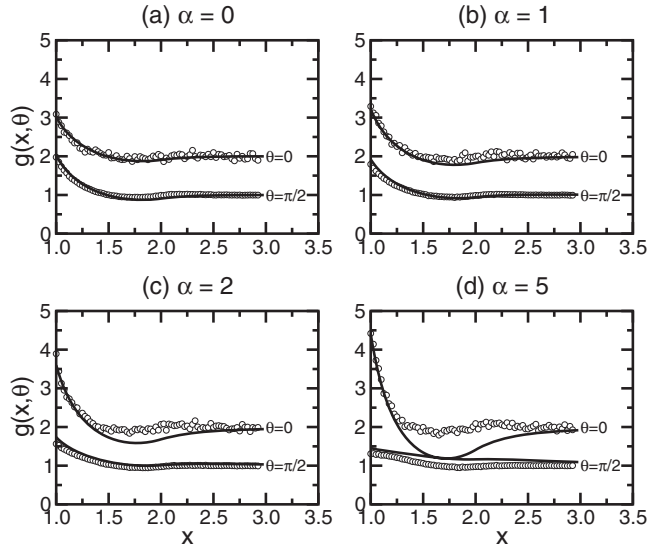

FIG. 5. Pair distribution functions $g(x, \theta)$ parallel to the field ($\theta = 0$, shifted along the ordinate by one unit, for clarity) and perpendicular to the field ($\theta = \pi/2$) in DHS fluids with $\varphi = 0.2$, $\lambda = 1$, and (a) $\alpha = 0$, (b) $\alpha = 1$, (c) $\alpha = 2$, and (d) $\alpha = 5$. The points are from simulations, and the lines are from theory.

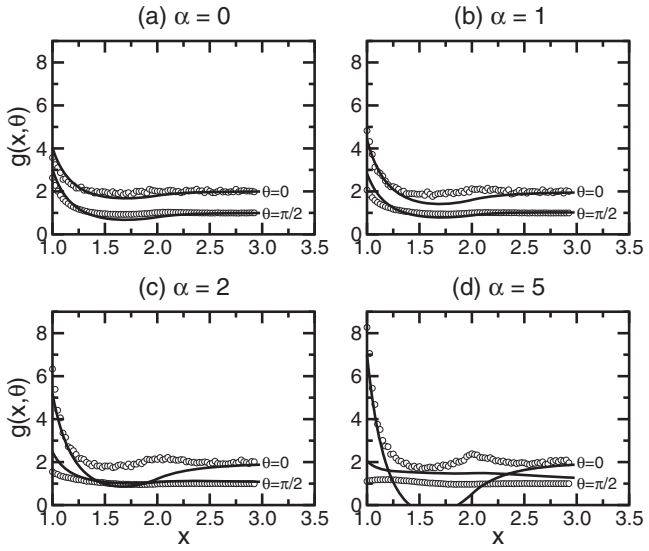

FIG. 6. Pair distribution functions $g(x, \theta)$ parallel to the field ($\theta = 0$, shifted along the ordinate by one unit, for clarity) and perpendicular to the field ($\theta = \pi/2$) in DHS fluids with $\varphi = 0.2$, $\lambda = 2$, and (a) $\alpha = 0$, (b) $\alpha = 1$, (c) $\alpha = 2$, and (d) $\alpha = 5$. The points are from simulations, and the lines are from theory.

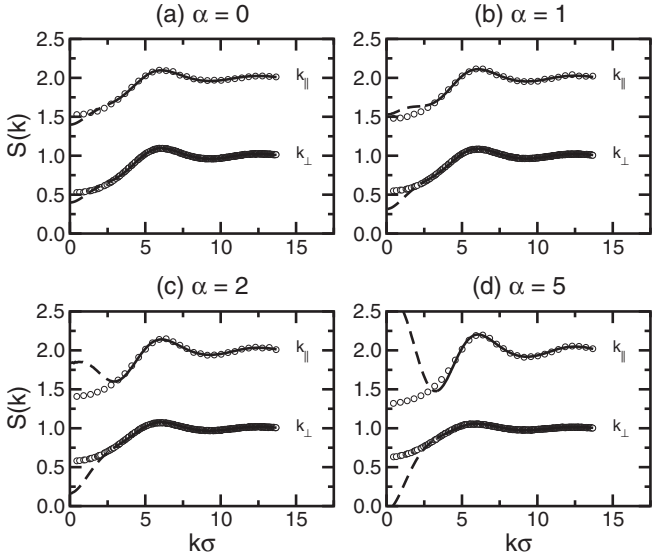

FIG. 7. Structure factors parallel to the field [$S(k_\parallel)$, shifted up one unit for clarity] and perpendicular to the field [$S(k_\perp)$] in DHS fluids with $\varphi = 0.1$ and $\lambda = 1$, and (a) $\alpha = 0$, (b) $\alpha = 1$, (c) $\alpha = 2$, and (d) $\alpha = 5$. The points are from simulations, and the lines are from theory with the unphysical regions highlighted with dashed lines.

of order $\varphi^2\lambda$, $\varphi^2\lambda^2$, etc., will be required to account for the PDF in the region of the first local minimum and the second peak. This is because the angle-averaged interactions will be relatively short ranged, and hence a sum of higher order terms in λ may be required to enhance the "attractive" second peak in the PDF. In strong fields, where the particles are strongly aligned, the effective interactions between particles are long ranged (r^{-3}) and hence it is possible that a single term of order $\varphi^2\lambda$ will be sufficient. In any case, four-body terms are difficult to evaluate, but this may be attempted in future work.

Dipolar coupling constants λ for real ferrofluids are rarely more than about 1. Volume fractions $\varphi \gtrsim 0.1$ are considered "concentrated," and in fact the range $\varphi = 0.01$–0.05 is more representative of materials used in applications and in optical measurements. Therefore, the parameters used here provide quite severe tests of the theory. For $\lambda = 1$ – certainly a typical value – the theory is quantitatively reliable except for the highest field strength ($\alpha = 5$) and highest volume fraction ($\varphi = 0.2$) considered in this work. In qualitative terms, theory and simulation show that short-ranged attractive correlations are enhanced in the field direction and reduced in a direction perpendicular to the field. Overall, these qualitative trends correlate well with those predicted by the early MSA theory for aligned DHSs.[17]

B. Structure factor $S(k)$

The structure factor $S(\boldsymbol{k})$ has been calculated for $\varphi = 0.01$–0.20, $\lambda = 1$ and 2, and $\alpha = 1$–5. Figure 7 shows the parallel and perpendicular structure factors $S(k_\parallel)$ and $S(k_\perp)$ for DHS fluids with $\varphi = 0.1$, $\lambda = 1$, and $\alpha = 0$, 1, 2, and 5. This state point corresponds to a moderately concentrated and strongly interacting ferrofluid. The purpose of this figure is to emphasize the extent to which the current level of theory describes the low-wavevector behavior in the structure factor. First, for wavevectors $k \gtrsim \pi$ (arising from pairs of particles at or near to contact) the agreement between theory and simulation is excellent. For lower wavevectors (corresponding to particles beyond the first coordination shell) the theory deviates from the simulation results. The problem is that the virial expansion is currently truncated at the three-body level. As explained in Sec. V A, the pair correlations mediated by more than one other particle are absent, and hence the decay of $g(\boldsymbol{r}_{12})$ beyond about 1.5σ (from Figs. 3–6) and the low-wavevector behavior of $S(\boldsymbol{k})$ will not be captured accurately. Of course, this also means that the thermodynamic equation of state – which can be linked through the isothermal compressibility to $S(0)$ – will be inaccurate, but it is expected that including terms of higher order in φ would improve matters.[36,43–45] The equation of state of the DHS fluid is currently under investigation.

It has been checked carefully that the low-wavevector anomalies in $S(\boldsymbol{k})$ are not artifacts arising from truncation errors or similar problems in the numerical Fourier transforms, which are best carried out in cylindrical polar coordinates.[41] Acknowledging this fundamental shortcoming of the theory, the unphysical regions in Fig. 7 are highlighted with dashed lines, and in what follows $S(\boldsymbol{k})$ will be truncated at the wavevector where an unphysical extremum or point of inflexion occurs.

Figure 8 shows $S(k_\parallel)$ and $S(k_\perp)$ for DHS fluids with $\lambda = 1$, volume fractions $\varphi = 0.01$–0.2, and $\alpha = 0$ and 5. As expected, the structure factors show more structure at higher volume fractions. Looking at the simulation results for $S(k_\parallel)$ first, upon application of a magnetic field the primary peak at $k_\parallel\sigma \simeq 2\pi$ increases and narrows due to the enhancement of near-neighbor nose-to-tail correlations in the field direction. The narrowing of the primary peak is in good correspondence with that seen in experimental[11–15] and previous simulation

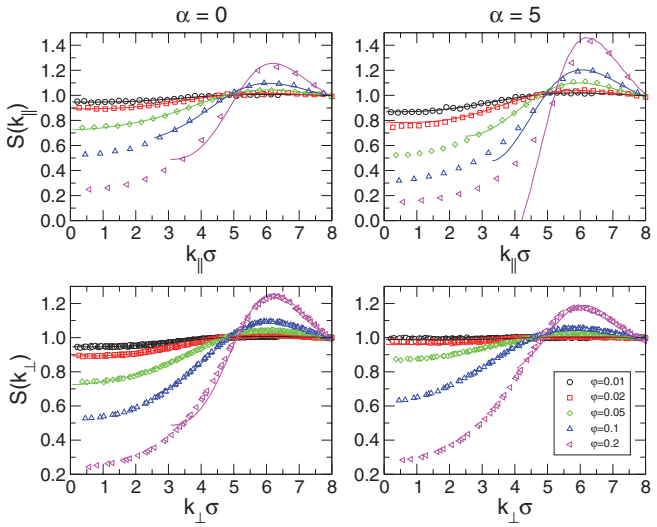

FIG. 8. Structure factors parallel to the field [$S(k_\parallel)$, top row] and perpendicular to the field [$S(k_\perp)$, bottom row] in DHS fluids with $\varphi = 0.01$–0.2, $\lambda = 1$, and $\alpha = 0$ (left column) and $\alpha = 5$ (right column). The points are from simulations, and the lines are from theory: (black circles and lines) $\varphi = 0.01$; (red squares and lines) $\varphi = 0.02$; (green diamonds and lines) $\varphi = 0.05$; (blue up triangles and lines) $\varphi = 0.1$; (magenta left triangles and lines) $\varphi = 0.2$.

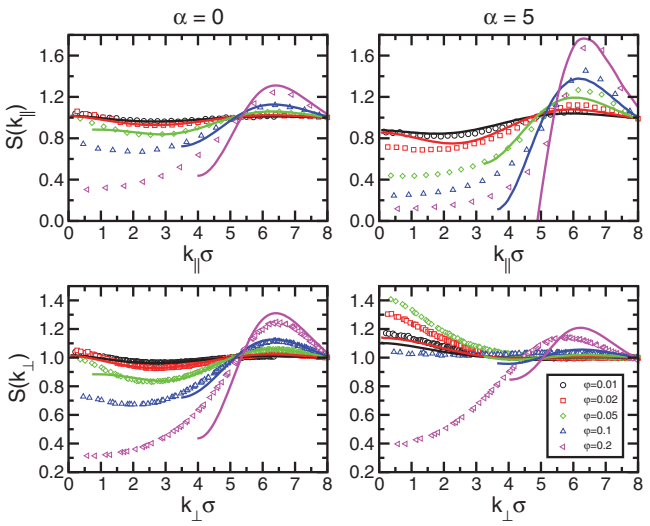

FIG. 9. Structure factors parallel to the field [$S(k_\parallel)$, top row] and perpendicular to the field [$S(k_\perp)$, bottom row] in DHS fluids with $\varphi = 0.01$–0.2, $\lambda = 2$, and $\alpha = 0$ (left column) and $\alpha = 5$ (right column). The points are from simulations, and the lines are from theory: (black circles and lines) $\varphi = 0.01$; (red squares and lines) $\varphi = 0.02$; (green diamonds and lines) $\varphi = 0.05$; (blue up triangles and lines) $\varphi = 0.1$; (magenta left triangles and lines) $\varphi = 0.2$.

studies.[20,22,23] For DHSs, the peak position does not shift because the distance of closest approach is fixed by the hard-sphere potential. The theory provides an excellent match with the simulation results at all volume fractions and for wavevectors that are not too low, as explained above; the primary peak and higher wavevector features of $S(k_\parallel)$ are well reproduced by the theory.

The perpendicular structure factor $S(k_\perp)$ shows a stronger dependence on the field, with the primary peak broadening and shifting to lower wavevector when the field is applied. The broadening of the primary peak correlates well with that seen in experimental[11–15] and previous simulation studies.[20,22,23] The shift is due to the parallel alignment of dipoles and the resulting repulsion between particles in a side-by-side configuration. This increases the near-neighbor separation in those configurations and hence a decrease in the corresponding wavevector. Another interesting feature is the decrease in the primary peak upon application of the field. The field-induced repulsions disfavor the side-by-side parallel configuration and hence the density of particles in this configuration decreases, leading to a smaller contribution to $S(k_\perp)$. As for the parallel structure factor, the theory does an excellent job of capturing the structural features seen in the simulations at all volume fractions, at least for wavevectors that are not too low.

The structure factors for DHS fluids with $\lambda = 2$, $\varphi = 0.01$–0.2, and $\alpha = 0$ and 5 are shown in Fig. 9. The primary peaks show the same trends as with $\lambda = 1$: in $S(k_\parallel)$ it increases in height and narrows; in $S(k_\perp)$ it decreases in height, broadens, and shifts to lower wavevectors. What is significantly different now, though, is the low-wavevector behavior of $S(k_\perp)$ measured in simulations which at low volume fractions $\varphi \leq 0.1$ shows a portion of negative slope in the range $k_\perp\sigma \lesssim \pi$.

To examine this feature more closely, Fig. 10 shows the low-wavevector sections of the perpendicular structure factor $S(k_\perp)$ in DHS fluids with $\varphi = 0.01$–0.1, $\lambda = 2$, and $\alpha = 5$, as measured in simulations. This behavior has been seen before.[20,23] In Ref. 20, Cerdà *et al.* concluded that, "At low volume fractions some long-range correlation seems to exist along the perpendicular direction that is induced by the magnetic field." In fact, this low-wavevector behavior is not due to long-range correlations, but rather to particles being positionally aligned along the field direction and the fluctuations of the particle positions from perfect alignment with the field. To demonstrate this, consider the simplest situation of an ideal equilibrium fluid of non-interacting monomers and

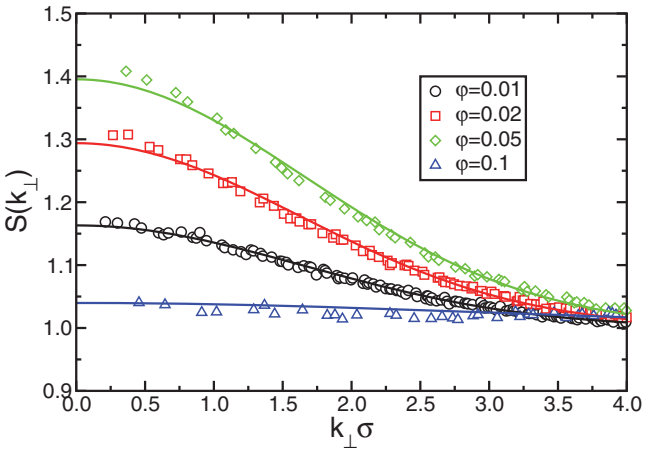

FIG. 10. Structure factor perpendicular to the field [$S(k_\perp)$] in DHS fluids with $\varphi = 0.01$–0.1, $\lambda = 2$, and $\alpha = 5$. The points are from simulations, and the lines are fits to the function $S(k_\perp) = 1 + a\exp(-bk_\perp^2)$: (black circles and line) $\varphi = 0.01$; (red squares and line) $\varphi = 0.02$; (green diamonds and line) $\varphi = 0.05$; (blue up triangles and line) $\varphi = 0.1$.

dimers in an applied field. The structure factor in this case was derived by Jordan:[16]

$$S(\boldsymbol{k}) = 1 - 2B_2\rho\xi(\boldsymbol{k}). \tag{37}$$

Here, B_2 is the second virial coefficient, and $\xi(\boldsymbol{k})$ is a function with the property that $\xi \to 1$ as $\boldsymbol{k} \to 0$, as required by the formal relationship $S(0) = \rho k_B T\kappa$,[36] where κ is the isothermal compressibility, and from the virial expansion $\rho k_B T\kappa = (1 + 2B_2\rho + \ldots)^{-1} \approx (1 - 2B_2\rho + \ldots)$. Jordan has provided expressions for ξ in various limits of the Langevin parameter α and the dipolar coupling parameter λ.[16] For the current purposes, it is sufficient to note that for wavevectors perpendicular to the field direction

$$\xi(k_\perp) = \exp\left[-(k_\perp\sigma)^2 f(\alpha, \lambda)\right], \tag{38}$$

where $f(\alpha, \lambda)$ is a function that depends on the particular regimes of α and λ. In simple terms, the statistics of the deviations in particle positions from perfect alignment with the field are Gaussian, and hence the structure factor – that measures density fluctuations – will also be Gaussian. The fact that there is a feature at low $k_\perp$ does not imply long-range correlations. Of course, the ideal monomer-dimer fluid is the simplest possible case, and the expressions provided by Jordan are approximate. Nonetheless, $S(k_\perp)$ does appear to be Gaussian, as shown by the fits of the form $[1 + a\exp(-bk_\perp^2)]$ included in Fig. 10. The structure factor increases in the range $\varphi = 0.01$–0.05 due to the growing proportion of correlated particles. It decreases between $\varphi = 0.05$ and 0.1 as the system develops in to a moderately concentrated fluid.

Returning to Fig. 9, it is clear that the virial-expansion theory is accurate for $S(k_\parallel)$ and $S(k_\perp)$ at moderate-to-high wavevectors. The theory does not quite capture the low-wavevector Gaussian behavior of $S(k_\perp)$ in high magnetic fields. This may be due to the magnetic interactions being captured only to order λ^2. The pair-interaction theory of Jordan, for example, is more successful on this particular point as it is a perturbation from the minimum-energy conformation of two interacting DHSs, rather than a perturbation theory starting from non-interacting DHSs.[16] There are other approaches which build upon the empirical observation that magnetic particles form chain-like clusters;[25–28] indeed, this is the only way to deal with strongly interacting magnetic particles that cluster even in the absence of an applied magnetic field. The current theory, however, is a systematic expansion that bridges the gap between non-magnetic and magnetic particles, and therefore is able to describe properly the significant interparticle correlations that occur even in the absence of distinct chain-like clusters. The current results are in good qualitative agreement with the early theories for DHSs of Jordan[16] and Hayter and Pynn.[17]

VI. CONCLUSIONS

The anisotropic pair correlations in models of ferrofluids in magnetic fields have been studied using a combination of statistical-mechanical theory and computer simulations. The PDFs have been calculated using a virial-expansion theory truncated at the three-body level and with the magnetic interactions included in a perturbative scheme to second order in the dipolar coupling constant. The comparison with accurate simulation data shows that the theory is reliable for realistic values of the dipolar coupling constant ($\lambda \sim 1$), volume fraction ($\varphi \leq 0.1$), and magnetic field strength. Significant deviations become apparent at high volume fractions, uncommonly high dipolar coupling constants, and very high field strengths. Overall, the theory does an excellent job in describing the anisotropy of the pair correlations in model ferrofluids with realistic parameters. It is emphasized once more that optical measurements of field-induced anisotropy in ferrofluids are carried out at such low volume fractions in order to gain sufficient optical transmission and to eliminate artifacts arising from multiple scattering.

The structure factors have also been calculated for wavevectors either parallel or perpendicular to the applied magnetic field. These functions pick out the differences in local structural inhomogeneity in the different directions. As with the pair distribution functions, the theory is basically reliable over realistic ranges of material parameters. For moderately concentrated fluids with strong interparticle interactions and in strong fields, the theory is less reliable at very low-wavevectors due to the many-body interactions that contribute to the long-range decay of the pair distribution functions, and which are omitted from the truncated virial-expansion theory. In addition, the theory does not capture the Gaussian density fluctuations perpendicular to the field that occur with high dipolar coupling constants, low volume fractions, and strong applied fields, and which arise from strongly correlated particles aligned nose-to-tail in the field direction.

The theory may of course be improved systematically by adding extra terms in the virial expansion. In the zero-field case, the coefficients β_{03} (equal to zero), β_{04}, β_{13}, and β_{14} of the terms of order λ^3, λ^4, $\varphi\lambda^3$, and $\varphi\lambda^4$, respectively, are already known.[19,20] The effects of adding these contributions to the PDF are negligible over the ranges of parameters studied here. This observation is quite surprising: it was anticipated that field-induced effects would lead to a perturbation of the zero-field PDF, and that it would therefore make sense to retain the higher order terms for which the field dependence has not yet been determined. The relative unimportance of these zero-field terms shows that the PDF undergoes a kind of crossover to high-field anisotropic behavior. This is actually quite encouraging, because it is now clear which terms should be determined next. The problems in the structure factor at low-wavevectors are due primarily to the omission of four-body (and higher) terms in the virial expansion and therefore the next most important term to be included should be of order $\varphi^2\lambda$, $\varphi^2\lambda^2$, etc.; this will be difficult, but it is possible in principle. Future work will concentrate on such higher order terms, and on the field-dependence of the terms β_{0n} and β_{1n} ($n \geq 3$).

Overall, the current theory provides a reliable means of predicting the degree and nature of anisotropic pair correlations in model ferrofluids in applied magnetic fields, with physically realistic parameters. The pair correlations dictate some of the most important physical properties of ferrofluids and represent essential information in the design and

synthesis of new functional materials. An in-depth knowledge of the microscopic structure of ferrofluids is therefore of the utmost importance in understanding and exploiting magnetic interactions in nanotechnology.

ACKNOWLEDGMENTS

E.A.E. and A.O.I. gratefully acknowledge grants from the Ministry of Education and Science of the Russian Federation (N2.609.2011) and the Russian Foundation for Basic Research (N10-02-00034-a). E.A.E. thanks the Ural Federal University for supporting a research visit to the University of Edinburgh where this work was completed.

[1]R. E. Rosensweig, *Ferrohydrodynamics* (Dover, New York, 1998).
[2]L. M. Pop and S. Odenbach, "Investigation of the microscopic reason for the magnetoviscous effect in ferrofluids studied by small angle neutron scattering," J. Phys.: Condens. Matter **18**, S2785 (2006).
[3]V. Socoliuc and L. B. Popescu, "The influence of long range interparticle correlations on the magnetically induced optical anisotropy in magnetic colloids," Physica A **390**, 569 (2011).
[4]V. Socoliuc and L. B. Popescu, "Extinction of polarized light in ferrofluids with different magnetic particle concentrations," J. Magn. Magn. Mater. **324**, 113 (2012).
[5]M. Zrínyi, L. Barsi, and A. Büki, "Deformation of ferrogels induced by nonuniform magnetic fields," J. Chem. Phys. **104**, 8750 (1996).
[6]M. Zrínyi, L. Barsi, D. Szabó, and H.-G. Kilian, "Direct observation of abrupt shape transition in ferrogels induced by nonuniform magnetic field," J. Chem. Phys. **106**, 5685 (1997).
[7]M. Zrínyi, "Intelligent polymer gels controlled by magnetic fields," Colloid Polym. Sci. **278**, 98 (2000).
[8]D. S. Wood and P. J. Camp, "Modeling the properties of ferrogels in uniform magnetic fields," Phys. Rev. E **83**, 011402 (2011).
[9]P. J. Camp, "The effects of magnetic fields on the properties of ferrofluids and ferrogels," Magnetohydrodynamics **47**, 123 (2011); online at http://mhd.sal.lv/contents/2011/2/MG.47.2.2.R.html.
[10]A. Yu. Zubarev, "On the theory of magnetic deformation in ferrogels," Soft Matter **8**, 3174 (2012).
[11]D. J. Cebula, S. W. Charles, and J. Popplewell, "The structure of magnetic particles studied by small angle neutron scattering," Colloid. Polym. Sci. **259**, 395 (1981).
[12]F. Gazeau, E. Dubois, J.-C. Bacri, F. Boué, A. Cebers, and R. Perzynski, "Anisotropy of the structure factor of magnetic fluids under a field probed by small-angle neutron scattering," Phys. Rev. E **65**, 031403 (2002).
[13]G. Mériguet, F. Cousin, E. Dubois, F. Boué, A. Cebers, B. Farago, and R. Perzynski, "What tunes the structural anisotropy of magnetic fluids under a magnetic field?" J. Phys. Chem. B **110**, 4378 (2006).
[14]J. Wagner, B. Fischer, and T. Autenrieth, "Field induced anisotropy of charged magnetic colloids: A rescaled mean spherical approximation study," J. Chem. Phys. **124**, 114901 (2006).
[15]A. Wiedenmann, U. Keiderling, M. Meissner, D. Wallacher, R. Gähler, R. P. May, S. Preévost, M. Klokkenburg, B. H. Erné, and J. Kohlbrecher, "Low-temperature dynamics of magnetic colloids studied by time-resolved small-angle neutron scattering," Phys. Rev. B **77**, 184417 (2008).
[16]P. C. Jordan, "Association phenomena in a ferromagnetic colloid," Mol. Phys. **25**, 961 (1973).
[17]J. B. Hayter and R. Pynn, "Structure factor of a magnetically saturated ferrofluid," Phys. Rev. Lett. **49**, 1103 (1982).
[18]L. B. Popescu and V. Socoliuc, "Perturbational statistical theories of magnetic fluids," J. Optoelectron. Adv. Mater. **7**, 3075 (2005); online at http://joam.inoe.ro/arhiva/pdf7_6/Popescu.pdf.
[19]E. A. Elfimova and A. O. Ivanov, "Pair correlations in magnetic nanodispersed fluids," J. Exp. Theor. Phys. **111**, 146 (2010).
[20]J. J. Cerdà, E. Elfimova, V. Ballenegger, E. Krutikova, A. Ivanov, and C. Holm, "Behavior of bulky ferrofluids in the diluted low-coupling regime: Theory and simulation," Phys. Rev. E **81**, 011501 (2010).
[21]S. Hess, J. B. Hayter, and R. Pynn, "A comparison of molecular dynamics and analytic calculation of correlations in an aligned ferrofluid," Mol. Phys. **53**, 1527 (1984).
[22]G. Mériguet, M. Jardat, and P. Turq, "Structural properties of charge-stabilized ferrofluids under a magnetic field: A brownian dynamics study," J. Chem. Phys. **121**, 6078 (2004).
[23]J. P. Huang, Z. W. Wang, and C. Holm, "Computer simulations of the structure of colloidal ferrofluids," Phys. Rev. E **71**, 061203 (2005).
[24]P. G. de Gennes and P. A. Pincus, "Pair correlations in a ferromagnetic colloid," Phys. Kondens. Mater. **11**, 189 (1970).
[25]J. M. Tavares, M. M. Telo da Gama, and M. A. Osipov, "Criticality of dipolar fluids: liquid-vapour condensation versus phase separation in systems of living polymers," Phys. Rev. E **56**, R6252 (1997).
[26]J. M. Tavares, J. J. Weis, and M. M. Telo da Gama, "Strongly dipolar fluids at low densities compared to living polymers," Phys. Rev. E **59**, 4388 (1999).
[27]A. O. Ivanov, S. S. Kantorovich, and E. S. Pyanzina, "Scaling behaviour of the structure factor of chain-forming ferrofluids at low wave vectors," Magnetohydrodynamics **44**, 33 (2008); online at http://mhd.sal.lv/contents/2008/1/MG.44.1.5.R.html.
[28]E. Pyanzina, S. Kantorovich, J. J. Cerdà, A. O. Ivanov, and C. Holm, "How to analyse the structure factor in ferrofluids with strong magnetic interactions: a combined analytic and simulation approach," Mol. Phys. **107**, 571 (2009).
[29]M. Klokkenburg, R. P. A. Dullens, W. K. Kegel, B. H. Erné, and A. P. Philipse, "Quantitative real-space analysis of self-assembled structures of magnetic dipolar colloids," Phys. Rev. Lett. **96**, 037203 (2006).
[30]P. J. Camp and G. N. Patey, "Structure and scattering in colloidal ferrofluids," Phys. Rev. E **62**, 5403 (2000).
[31]T. Tlusty and S. A. Safran, "Defect-induced phase separation in dipolar fluids," Science **290**, 1328 (2000).
[32]G. Ganzenmüller, G. N. Patey, and P. J. Camp, "Vapour-liquid phase transition of dipolar particles," Mol. Phys. **107**, 403 (2009).
[33]L. Rovigatti, J. Russo, and F. Sciortino, "No evidence of gas-liquid coexistence in dipolar hard spheres," Phys. Rev. Lett. **107**, 237801 (2011).
[34]L. Rovigatti, J. Russo, and F. Sciortino, "Structural properties of the dipolar hard-sphere fluid at low temperatures and densities," Soft Matter (in press).
[35]E. Elfimova and A. Ivanov, "The radial distribution function and the structure factor of dipolar hard spheres," Magnetohydrodynamics **44**, 39 (2008); online at http://mhd.sal.lv/contents/2008/1/MG.44.1.6.R.html.
[36]J.-P. Hansen and I. R. McDonald, *Theory of Simple Liquids*, 3rd ed. (Academic, London, 2006).
[37]A. O. Ivanov, S. S. Kantorovich, E. N. Reznikov, C. Holm, A. F. Pshenichnikov, A. V. Lebedev, A. Chremos, and P. J. Camp, "Magnetic properties of polydisperse ferrofluids: A critical comparison between experiment, theory, and computer simulation," Phys. Rev. E **75**, 061405 (2007).
[38]A. O. Ivanov, S. S. Kantorovich, E. N. Reznikov, C. Holm, A. F. Pshenichnikov, A. V. Lebedev, A. Chremos, and P. J. Camp, "Magnetic measurements as a key for the particle size distribution in ferrofluids: experiment, theory, and computer simulations," Magnetohydrodynamics **43**, 393 (2007); online at http://mhd.sal.lv/contents/2007/4/MG.43.4.2.R.html.
[39]J. E. Mayer and E. Montroll, "Molecular distribution," J. Chem. Phys. **9**, 2 (1941).
[40]J. de Boer, "Molecular distribution and equation of state of gases," Rep. Prog. Phys. **12**, 305 (1949).
[41]Yu. A. Buyevich and A. O. Ivanov, "Equilibrium properties of ferrocolloids," Physica A **190**, 276 (1992).
[42]M. P. Allen and D. J. Tildesley, *Computer Simulation of Liquids* (Clarendon, Oxford, 1987).
[43]C. G. Joslin, "The third dielectric and pressure virial coefficients of dipolar hard sphere fluids," Mol. Phys. **42**, 1507 (1981).
[44]C. Joslin and S. Goldman, "The third dielectric and pressure virial coefficients of dipolar hard sphere fluids ii. numerical results," Mol. Phys. **79**, 499 (1993).
[45]D. Henderson, "Second virial coefficient for the dipolar hard sphere fluid," J. Chem. Phys. **135**, 044514 (2011).